X-ray grazing incidence diffraction from polycrystalline Sb films on single-crystal substrates



1993 J. Phys.: Condens. Matter 5 8149

(http://iopscience.iop.org/0953-8984/5/44/008)

J. Phys.: Condens. Matter 5 (1993) 8149–8158. Printed in the UK

# X-ray grazing incidence diffraction from polycrystalline Sb films on single-crystal substrates

E Findeisen†, L Brügemann, J Stettner and M Tolan

Institut für Experimentalphysik, Christian-Albrechts-Universität Kiel, Leibnizstraße 19, D-24098 Kiel, Federal Republic of Germany

Received 15 February 1993, in final form 19 August 1993

**Abstract.** The intensity of Bragg reflections depends strongly on the angle of incidence, if a highly collimated beam of x-rays is impinging at grazing incidence on a thin (200–600 Å) polycrystalline antimony layer. In the case of asymmetric grazing incidence diffraction (AGID) the angle of incidence is small, as the exit angle must be large and nearly twice the Bragg angle. The experimental data are analysed on the basis of the distorted wave born approximation (DWBA), which yields the thickness $d$ and the optical constants $\delta$ and $\beta$ of the layer. These parameters are compared with those determined from total external reflection data.

## 1. Introduction

Grazing incidence diffraction (GID) techniques have been widely employed to study near surface properties of crystals and liquids (see, e.g., [1–5]). There have been extensive efforts to calculate the measured Bragg intensities from single crystals (a summary is given by Dosch in [6]), which represent the case of coherent scattering. Incoherent scattering also has been studied, with the example of thermal diffuse scattering [7]. A question exists as to whether GID is a competitive surface sensitive technique for the study of polycrystalline films (of thicknesses of several hundred Ångstroms). We have attempted such experiments in an asymmetric set-up with the incoming beam at a small angle $\alpha_i$ that is of the order of the critical angle $\alpha_c$ (in an extended range up to 10°), and the scattered beam at large angles $\alpha_f$, of the order of $2\Theta_B$ ($\Theta_B$ is the Bragg angle). This geometry (asymmetric grazing incidence diffraction, AGID) is considered in Vineyard's theoretical approach [8], which provides an analysis of the scattered intensity in terms of the so called distorted wave born approximation (DWBA). As it turns out, the analysis requires a reasonably good understanding of the texture of the sample. Therefore the grazing incidence experiments have been complemented by a (partial) determination of the texture.

In a previous work Huang analysed the structure and depth profiles of ultrathin $Fe_2O_3$ films [9]. In contrast to this publication, the present work concentrates on the explanation of the diffracted intensity in terms of the DWBA, with less emphasis on the specific example.

The calculation of the diffuse scattering from rough surfaces in the range of total external reflection ($\alpha_i \simeq \alpha_c$ and $\alpha_f \simeq \alpha_c$) is another well known application of the DWBA [10–13], but it is not the subject of this paper.

† Present address: Risø National Laboratory, DK-4000 Roskilde, Denmark.

0953-8984/93/448149+10$07.50 

## 2. Samples

The Sb films were prepared by evaporation from a Knudsen cell onto either Si(111) or cleaved GaAs(110) substrates in an ultrahigh-vacuum (UHV) chamber (base pressure $< 10^{-9}$ Pa). Before evaporating, the Si(111) substrate was cleaned with acetone and heated within the UHV chamber for 45 min at a temperature of 1070 K. The thicknesses of the layers have been determined approximately by the frequency shift of a quartz thickness monitor (see table 1.). This method is rather inaccurate, since the sticking coefficients of GaAs and the oscillating crystal are quite different. The x-ray measurements were not performed under vacuum conditions.

**Table 1.** Sample preparation: the thicknesses are determined by a quartz thickness monitor.

| Sample | Deposition time (min) | Thickness (Å) |
|---|---|---|
| Sb/Si | 10 | 250 |
| Sb/GaAs | 25 | 270 |

The Sb layers are polycrystalline, but may have a pronounced texture. The crystal structure of Sb is rhombohedral with the space group $R\bar{3}m$ and the hexagonal lattice constants are $a = 4.307$ Å and $c = 11.273$ Å [14].

A texture modifies the dependence of the intensity on the angle of incidence. Therefore it has to be checked whether the crystallites are randomly oriented. Random orientation only was found for the Sb/Si sample. Sb/GaAs, however, has a [0 1 20] fiber texture [15], i.e. the [0 1 20] direction of each crystallite is normal to the surface of the substrate. We were unable to take complete pole figures, because the geometry of the instrument restricts the accessible part of the reciprocal space. To determine the position of the 006 reflection, extended scans with four different sample orientations were performed. In all cases an angle of 8° was measured between the surface normal and the positions of the 006 reflection. We attempted to compensate the geometrical restrictions by investigating the positions of other reflections (012, 104, 015, 107, 116, 018, 009 and 119). All results agree with the model of a [0 1 20] fiber texture. The cylindrical symmetry (fiber texture) has no simple explanation, e.g. by a miscut of the substrate, and a complete interpretation is still missing.

## 3. Experimental set-up

The x-ray source is a 12 kW x-ray generator with a rotating copper anode. The Cu K$\alpha$ line is extracted by use of Bragg reflection from a flat Ge(111) crystal as monochromator. Slits of dimension $2\times0.3$ mm$^2$ in front of and $10\times0.2$ mm$^2$ behind the monochromator limit the divergence of the beam so that only the K$\alpha_1$ part of the Cu radiation with a wavelength of $\lambda = 1.54056$ Å reaches the sample, which was mounted on a two-circle goniometer (the incident angle $\alpha_i$ and the scattering angle $\alpha_f$ can be varied, see figure 1). The scattered intensity is detected with a linear position sensitive detector (PSD), which uses argon/methane as a counter gas. It has a spatial resolution of about 35 $\mu$m. At a distance of 30 cm from the sample the PSD accepts the scattered radiation within an angular range of 7°.

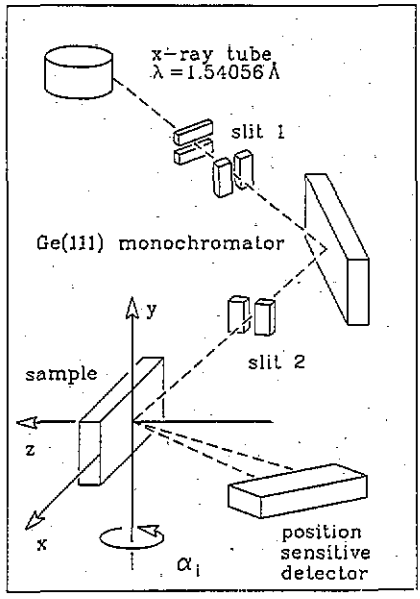


**Figure 1.** Schematic geometry of an AGID experiment.

## 4. Theory

The theoretical description is based on the DWBA, as treated by Vineyard [8]. The DWBA consists of two steps.

The basic idea of GID is that the penetration depth of the electric field in the region of total external reflection is only about 50 Å. In this region multiple scattering dominates. Hence for the interpretation a dynamical treatment as the *first* step of the DWBA is needed. The calculation of the distorted wave inside the layer is carried out exactly for the approximation of a homogeneous dielectric medium that can be described by the refractive index $n' = 1 - \delta - i\beta$.

The *second* step of the DWBA includes the scattering from the periodic atomic structure of the layer and can be performed within a kinematical approach. In the following section both steps of the DWBA are outlined. An extensive summary of the use of the DWBA is given by Dosch [6].

### *4.1. Dynamical calculation of the distorted wave*

A plane, linearly polarized electromagnetic wave $\mathcal{E} = \boldsymbol{E} \exp[i(\boldsymbol{k} \cdot \boldsymbol{r} - \omega t)]$ impinges on the smooth surface of the sample (see figure 2). $\boldsymbol{k}$ denotes the incident wavevector with $|\boldsymbol{k}| = k = 2\pi/\lambda$. The change of the refractive index at the surface causes a refracted wave $\mathcal{E}'$ with the wavevector $\boldsymbol{k}'$ and the amplitude $\boldsymbol{E}'$ (primes denote quantities within the film). $\alpha_i'$ denotes the angle of refraction. By using Maxwell's equations and the boundary conditions at $z = 0$, the wavevector $\boldsymbol{k}'$ and the electric field $\mathcal{E}'$ within the sample can be calculated [8] (see also figure 2):

$$\boldsymbol{k}' = k \begin{pmatrix} \cos\alpha_i \\ 0 \\ -\sqrt{n'^2 - \cos^2\alpha_i} \end{pmatrix} \tag{1}$$

$$\boldsymbol{E}' = \begin{pmatrix} 2|k_z'|/(n'^2 k_z + |k_z'|) & 0 & 0 \\ 0 & 2k_z/(k_z + |k_z'|) & 0 \\ 0 & 0 & 2k_z/(n'^2 k_z + |k_z'|) \end{pmatrix} \boldsymbol{E}. \quad (2)$$

The components of equation (2), when expressed in more elementary terms for the cases of parallel and perpendicular polarization, are also known as Fresnel's equations. Using equation (2), the transmission coefficient $|T_i|^2 = |\boldsymbol{E}'|^2/|\boldsymbol{E}|^2$ for an unpolarized beam impinging on a smooth surface is given by (see also figure 2)

$$|T_i|^2 = (\sin^2\alpha_i/2)|2|k_z'|/(n'^2 k_z + |k_z'|)|^2 + \tfrac{1}{2}|2k_z/(k_z + |k_z'|)|^2 + (\cos^2\alpha_i/2)|2k_z/(n'^2 k_z + |k_z'|)|^2. \quad (3)$$

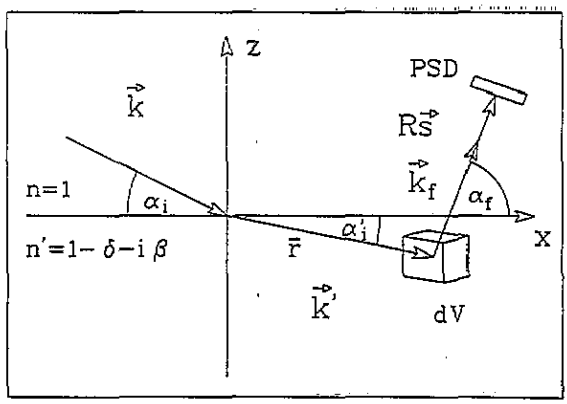


**Figure 2.** Refraction of a plane wave $k$ and scattering of the distorted wave $k'$ by the volume element $dV$ at the air/layer interface ($z = 0$). $k_f$ denotes the scattered wavevector. The angles $\alpha_i$ and $\alpha_i'$ are greatly exaggerated.

### *4.2. Kinematical treatment of the scattering process*

In the second step of the DWBA the distorted wave is considered to illuminate the scatterer. The kinematical approach is equivalent to a Born approximation with the distorted wave taken as the incident wave.

- The neglect of multiple scattering is justified because the scattered wave amplitude $E_f$ is small compared with the amplitude $E'$ of the distorted wave ($E_f/E' \simeq 10^{-2}$–$10^{-3}$). The index f denotes quantities after the scattering process.
- The reflection at the layer/substrate interface can be neglected, too, because the critical angle of total external reflection of Sb is larger than the critical angle of the substrate. Hence there is little reflection at this interface.
- Finally, the refraction and reflection of the *scattered* wave at the layer/air interface can be neglected, because the exit angle is very large (i.e. $\alpha_f = 20°$–$40°$). Therefore $|T_f|^2 \simeq 1$ can be taken. On the other hand refraction corrections are of importance if $\alpha_f$ is in the range of $\alpha_c$ [7].

The basic equation in Vineyard's paper for the calculation of the scattered wave at a distance point $R\,s$ is (see figure 2) [8]

$$\mathcal{E}_f = \mathcal{E}_{el} \sum_n f_n(\boldsymbol{Q}) \exp(-i\,\boldsymbol{Q}\cdot\boldsymbol{r}_n). \tag{4}$$

Here $s$ is the unit vector in the direction of the scattered beam, $r_n$ is the position and $f_n(\boldsymbol{Q})$ the structure factor of the $n$th atom. $\boldsymbol{Q} = \boldsymbol{k}_f - \boldsymbol{k}'$ denotes the scattering vector inside the layer. The summation in equation (4) must be performed over all atoms of the film. Then the electric field $\mathcal{E}_{el}$ of a single electron excited by the distorted wave (in cgs units) is

$$\mathcal{E}_{el} = \left(e^2/mc^2R\right) \exp(-i\omega t) E'_\perp \tag{5}$$

where $\boldsymbol{E}'_\perp$ denotes the part of $\boldsymbol{E}'$ lying in the plane perpendicular to $\boldsymbol{k}_f$.

Calculating the Poynting vector yields the intensity at $R\,s$ which is $I_f = (c/8\pi)|\mathcal{E}_f|^2$. Unfortunately $I_f$ is very difficult to obtain in the experiment because an extremely high resolution is required. We now turn to a more useful quantity, the integrated intensity $P$, obtained by integrating $I_f$ over the area of the illuminated volume, properly accounting for the number of crystallites fulfilling the Bragg condition [16]. For each reflection the integrated intensity is proportional to $|\mathcal{E}'|^2$ (i.e. to the intensity that excites the scattering electrons) and also to the scattering volume element $\mathrm{d}V$

$$P \propto \int |\mathcal{E}'|^2 \,\mathrm{d}V. \tag{6}$$

This is not correct for crystallites having a diameter comparable to the scattering depth, because the damping of the electric field within the crystallite has to be taken into account. Hence we have a certain phase relation between the waves scattered by two different electrons. Accordingly, for the calculation of the intensity scattered by one crystallite we have to proceed in the following manner: first the waves scattered by all electrons in a crystallite have to be summed up and then the square of the electric field must be taken. This can be carried out exactly and leads to the same expression (6) for the integrated intensity. Therefore both cases, the intensity from different crystallites and the superposition of waves scattered from electrons of the same crystallite, can be described by equation (6).

The integration in equation (6) must be performed over the whole scattering volume $V = A\,d$. Here $A$ is the illuminated surface area of the sample and $d$ is the thickness of the Sb layer. Other quantities influencing $P$ are of no interest, since they do not depend on the angle of incidence $\alpha_i$. Defining the scattering depth $l$ ($\mathrm{Im}(k'_z)$ denotes the imaginary part of the complex quantity $k'_z$)

$$l := \left\{1 - \exp\left[2\,d\,\mathrm{Im}\left(k'_z\right)\right]\right\} / \left[-2\,\mathrm{Im}\left(k'_z\right)\right] \tag{7}$$

we find, after carrying out the integration in equation (6) and dividing by the incident intensity

$$P_{norm} \propto A\,|T_i|^2\,l \tag{8}$$

for the normalized integrated intensity of a reflection $h\,k\,l$. With the definition of $l$ given in equation (7) the area beneath the curve $|\mathcal{E}'(z)|^2$ can be represented by a box of height $|\boldsymbol{E}'|^2 = |\mathcal{E}'(z=0)|^2$ and length $l$:

$$l|\boldsymbol{E}'|^2 = \int_{-d}^{0} |\mathcal{E}'|^2 \mathrm{d}z. \tag{9}$$

The slight difference between equation (7) and Vineyard's corresponding definition for a semi-infinite medium disappears in the limit of $d \to \infty$.

The dependence of the illuminated area $A$ on $\alpha_i$ is a purely geometrical effect, because only for small angles the x-ray beam strikes the whole sample. For larger incident angles, $A$ becomes smaller and we have ($h_{sample}$ is the height of the sample and $b_{beam}$ the width of the x-ray beam at the sample position) $A = h_{sample} b_{beam} / \sin\alpha_i$.

Below, we show that equation (8) describes the measurements satisfactorily.

## 5. Measurements and discussion

The 012, 104 and 003 reflections of Sb belong to those with the highest intensities. The respective intensities of the 104 and 003 reflection are 70% and 25%, compared to the intensity of the 012 reflection [14]. For the sample Sb/Si(111) the intensity of the 012 and 104 reflection was investigated. For the other sample, Sb/GaAs(110), only the (003) reflection was observable at grazing incidence because of a strong texture of the Sb crystallites.

The angular position of the PSD was chosen to be twice the Bragg angle of the reflection *hkl*. Then the sample was rotated from $\alpha_i = 0.1°$ up to $\alpha_i = 10°$, with a counting time of 1 h for each angle $\alpha_i$. The PSD recorded the diffracted intensity within a range of 7° in the scattering plane. In the perpendicular direction the PSD was wide open and collects a constant fraction of the intensity of the diffraction cone that corresponds to the *hkl* reflection of the powder. The integrated intensity $P$ can be obtained after subtracting the background and integrating over the $\alpha_f$ range of the reflection. $P$ as a function of the incident angle $\alpha_i$ is represented on a double logarithmic scale in order to emphasize the most interesting part of the curve (i.e. small $\alpha_i$ values).

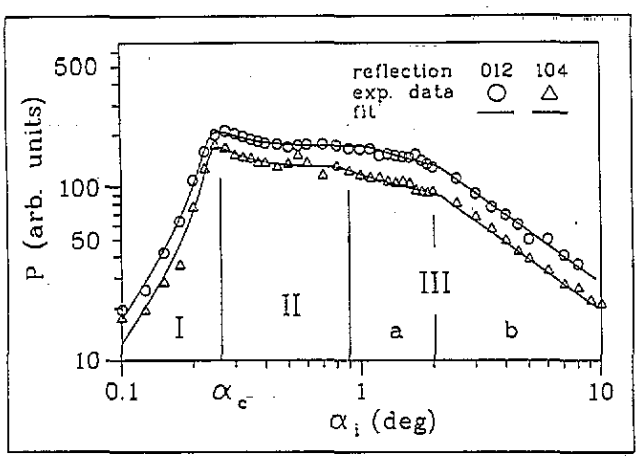


**Figure 3.** The experimental results for two different reflections 012 and 104 of the sample Sb/Si(111) are compared with the calculation (solid curves) according to equation (8). The different ranges of the curves (I–III(b)) are explained in the text.

Three different ranges of the curve can be easily distinguished (see figure 3).

(I) The first section $0 < \alpha_i \simeq \alpha_c$ is dominated by the increase of both the scattering depth $l$ and the transmission coefficient $|T_i|^2$ (see figure 4). The maximum of the transmission function $|T_i|^2$ at $\alpha_i \simeq \alpha_c$ is not very pronounced.

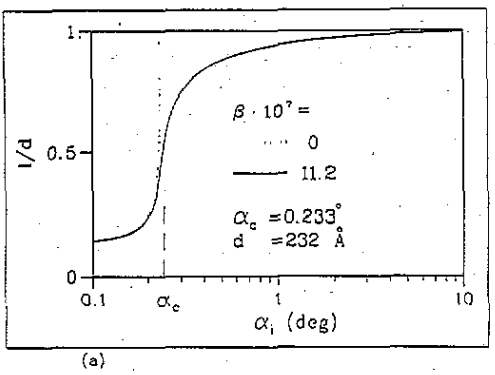


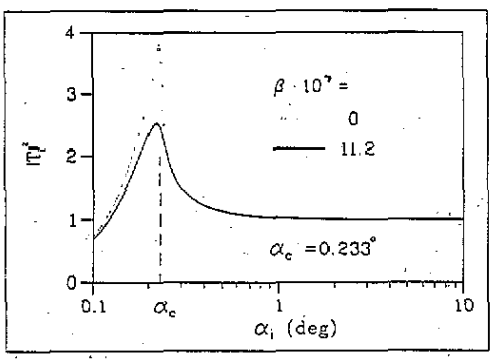


**Figure 4.** (*a*) The scattering depth $l$ compared with the thickness of the layer $d$ and (*b*) the Fresnel transmissivity $|T_i|^2 = |E^t|^2/|E|^2$ both as a function of the angle of incidence $\alpha_i$ for a transparent medium and for the real system Sb/Si(111) with $d = 232$ Å, $\alpha_c = 0.233° \simeq \sqrt{2\delta}$, and $\beta = 11.2 \cdot 10^{-7}$ (see table 2).

**Table 2.** Results of the least-squares fits for the data of both samples. $d$ is the thickness, $\delta$ and $\beta$ the optical constants of the Sb layer.

| | Sb/Si | | Sb/GaAs |
|---|---|---|---|
| | 012 | 104 | 003 |
| $d$ (Å) | 232 ± 18 | 229 ± 30 | 524 ± 65 |
| $\beta \times 10^7$ | 11.2 ± 1.0 | 9.2 ± 1.7 | 19.7 ± 1.5 |
| $\delta \times 10^6$ | 8.3 ± 0.3 | 8.6 ± 0.5 | 16.9 ± 0.6 |
| dx (mm) | 0.040 ± 0.004 | 0.049 ± 0.005 | 0.027 ± 0.005 |

(II) For angles $\alpha_i > \alpha_c$, but not too large, the electric field already decreases, whereas the scattering depth still increases and the intensity does not vary very much.

(III) Above a certain angle the x-ray beam no longer illuminates the whole sample. The reduction of $A$ is proportional to $1/\sin\alpha_i$. Due to the logarithmic scale we have an approximately linear relation, that is $\log A \simeq -\log\alpha_i +$ constant.

The particular shape of the curve in figure 3 is reproduced perfectly well by equation (8). From fits to each curve we obtain the thickness $d$ and the optical constants $\beta = \mu/2k$ and $\delta = 1 - \cos(\alpha_c)$ of the antimony film ($\mu$ denotes the linear absorption coefficient of the

film). The fit results are listed in table 2.

Other parameters which were used in the fit procedure are of minor physical interest: (i) the width of the sample ($b_{sample} \simeq 10$ mm), (ii) the width of the beam ($b_{beam} \simeq 0.25$ mm) and (iii) the displacement d$x$ (see below and table 2). As the width of the second slit is 0.2 mm, the fitted value of $b_{beam}$ seems to be reasonable.

The agreement between measured and calculated intensities can be improved by introducing a displacement d$x$, which describes an eventual displacement of the sample from the middle of the beam. This introduces an asymmetry, considering the illuminated part of the sample surface (in particular see figure 3, ranges III(a) and III(b)).

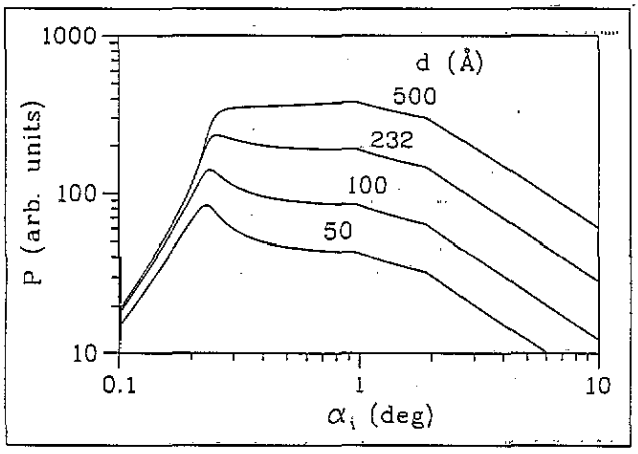


**Figure 5.** The integrated intensity $P(\alpha_i)$ is calculated for various values of $d$ and for fixed $\beta = 11.2 \times 10^{-7}$.

The influence of the parameter $d$ on the calculated intensity in equation (8) is demonstrated in figure 5. Increasing $\beta$ (i.e. increasing absorption) of the film leads to a reduced size of the peak in $T_i$.

**Table 3.** A comparison of the data obtained by total external reflection measurements of the specular beam and AGID. $d$ is the thickness of the layer and $\delta$ the optical constant associated with the real part of the refractive index $n' = 1 - \delta - i\beta$.

| | Sb/Si | | Sb/GaAs | |
|---|---|---|---|---|
| | $d$ (Å) | $\delta \times 10^6$ | $d$ (Å) | $\delta \times 10^6$ |
| Total reflection | 245 ● 14 | $8.0 \pm 0.6$ | $563 \pm 1$ | $18.4 \pm 0.2$ |
| AGID | $231 \pm 24$ | $8.5 \pm 0.4$ | $524 \pm 65$ | $16.9 \pm 0.6$ |

The parameters $d$ and $\delta$ are also accessible by total external reflection measurements (see table 3).

The thicknesses determined by the reflectivity in the range of total external reflection are close to those measured by AGID. On the other hand, the thickness of the Sb layer on GaAs measured by x-rays in this work is more than twice the value determined by the quartz thickness monitor (see table 1). This is surprising as the sticking coefficient of a cleaved GaAs(110) surface should be much lower than that of the monitor. An explanation for this fact is still missing here, however.

## 6. Conclusion

A rather precise interpretation, based on the DWBA of the intensity profile of AGID measurements as a function of $\alpha_i$ has been generated.

Concerning the particular substances investigated in this work there is a marked difference between Sb on Si(111) and on GaAs(110). In the case of Sb on GaAs(110) there is a pronounced texture. The density, which is associated with the optical constant $\delta$, is close to that of bulk Sb. Sb on Si(111) on the other hand has no measurable texture. The lack of a well defined modulation in the reflectivity curves can be explained by an inhomogeneous layer. More specifically, the reduced density of the film only 50% of the bulk value (see table 3), signals an island formation. In this context it appears surprising, that the peak close to $\alpha_c$ in the AGID measurements is more pronounced for Sb on Si(111), which seems to have the less well defined surface. One possible explanation is that the thickness of the Sb layer on GaAs is more than twice of the film thickness on the Si substrate. Therefore the increased scattering depth yields a higher integrated intensity in the case of Sb/GaAs (especially in the ranges II and III of figure 3, where $\alpha_i > \alpha_c$; see also figure 5). Another possible explanation is given by the increase of the transmission $T_i$ with increasing roughness of the surface as proposed by Weber and Lengeler [13]: the transmission coefficient $T_i^r$ of a rough surface with roughness $\sigma$ ($\sigma$ denotes the root mean square roughness of a Gaussian random height distribution) is [17, 13]

$$T_i^r = T_i \exp\left[+\tfrac{1}{2}\sigma^2(k_z - k_z')^2\right]. \tag{10}$$

For the shape of $P(\alpha_i)$ calculated following equation (8), two extreme cases can be distinguished. If the film is very thin, $P(\alpha_i)$ is determined by $T_i(\alpha_i)$. On the other hand, for thick films the factor $l(\alpha_i)$ dominates. This is demonstrated in figure 8 of the publication by Huang [9]. This figure shows the integrated intensities of the reflections of a 90 Å thin $\alpha$-$Fe_2O_3$ layer on top of a very thick (several $\mu$m) layer of $\gamma$-$Fe_2O_3$ up to $\alpha_i = 0.7°$. The integrated intensities for our sample Sb on Si(111) with $l(\alpha_i = \alpha_c)/d \simeq 0.5$ (figure 4(a)) show the influence of both components within a range of $\alpha_i$ up to 10°.

## Acknowledgments

The authors would like to thank H Carstensen for preparation of the samples and W Press and J M Gay (CRMC2, Marseille) for many stimulating and helpful discussions. The support by the Bundesministerium für Forschung und Technologie under contract No. 03 PR3 KIE9 is gratefully acknowledged.

## References

[1] Dosch H, Battermann B W and Wack D C 1986 *Phys. Rev. Lett.* **56** 1144
[2] Kjaer K, Als-Nielsen J, Helm C A, Laxhuber L A and Möhwald H 1987 *Phys. Rev. Lett.* **58** 2224
[3] Grotehans S, Wallner G, Burkel E, Metzger H, Peisl J and Wagner H 1989 *Phys. Rev.* B **39**, 8450
[4] Segmüller A 1991 *J. Vac. Sci. Technol.* A **9** 2477
[5] Hong H, Aburano R D, Lin D-S, Chen H, Chiang T-C, Zschack P and Specht E D 1992 *Phys. Rev. Lett.* **68** 507
[6] Dosch H 1992 *Critical Phenomena at Surfaces and Interfaces* (Berlin: Springer)
[7] Dosch H 1987 *Phys. Rev.* B **35** 2137
[8] Vineyard G H 1982 *Phys. Rev.* B **26** 4146

[9] Huang T C 1990 *Adv. X-Ray Anal.* **33** 91
[10] Sinha S K, Sirota E B, Garoff S and Stanley H B 1988 *Phys. Rev.* B **38** 2297
[11] Pynn R 1992 *Phys. Rev.* B **45** 602
[12] Bahr D, Press W, Jebasinski R and Mantl S 1993 *Phys. Rev.* B **47** 4385
[13] Weber W and Lengeler B 1992 *Phys. Rev.* B **46** 7953
[14] McClune W F (ed) 1985 *Powder Diffraction File, Inorganic Phases* (Swarthmore, PA: International Centre of Diffraction Data)
[15] Findeisen E 1992 *Diplomarbeit* Christian-Albrechts-Universität Kiel
[16] Warren B E 1969 *X-ray Diffraction* (Reading, MA: Addison-Wesley)
[17] Vidal B and Vincent P 1984 *Appl. Opt.* **23** 1794